Casimir effect in critical films of binary liquid mixtures

Ashis Mukhopadhyay and Bruce M. Law
Condensed Matter Laboratory, Department of Physics, Kansas State University, Manhattan, Kansas 66506-2601
(Received 20 October 1999; revised manuscript received 25 April 2000)

We present experimental evidence for the Casimir effect within critical films of binary liquid mixtures possessing opposite boundary conditions $(+-)$ by studying the thickness of these vapor-adsorbed films on a silicon wafer as a function of temperature near the critical temperature. Our results for two different critical mixtures demonstrate that the critical Casimir pressure scaling function $\vartheta^{+-}(y)$ scales with $y=L/\xi$, where L is the equilibrium film thickness and ξ is the bulk correlation length. Additionally, on approaching the critical temperature T_c an increase in the film thickness L is observed, implying that the sign of the universal Casimir amplitude $\Delta^{+-}=\vartheta^{+-}(0)/2$ at T_c is positive, consistent with theoretical predictions. However, the magnitude of the Casimir amplitude that we measure is approximately two orders of magnitude smaller than that given by prevailing theories. In the two-phase region of the liquid mixture, preliminary evidence suggests that the adsorbed film undergoes a surface phase transition from a film near the critical composition at $T \lesssim T_c$ to a film near one of the bulk phases at $T \ll T_c$. This low temperature film composition most likely corresponds to the bulk phase rich in the component that preferentially adsorbs at the silicon surface.

PACS number(s): 05.70.Jk, 68.35.Rh, 64.60.Fr, 68.15.+e

I. INTRODUCTION

The interaction between macroscopic bodies, even if they are uncharged, is primarily electromagnetic in nature. This interaction in general depends upon the dielectric properties of the bodies and the intervening medium and also on the geometric size and shape of the bodies and the separation distance between them. Casimir [1] first showed that two uncharged perfectly conducting plates placed parallel to each other in vacuum experience an attractive force proportional to the inverse fourth power of their separation (L). The force originates because the zero-point fluctuations of the electromagnetic field between the plates have to satisfy appropriate boundary conditions at the plates; these boundary conditions modify the frequency spectrum in such a way that the energy of the electromagnetic field exhibits an L dependence. The derivative of this energy with respect to L can be interpreted as an effective force acting between the plates, which is known as the Casimir force. Lifshitz [2] generalized the ideas of Casimir to a vacuum between two dielectric plates at finite temperatures by considering the free energy instead of the zero-point energy. Dzyaloshinskii, Lifshitz, and Pitaevskii (DLP) [3] later provided a more comprehensive theory for a dielectric fluid confined between dielectric plates. The DLP theory for dispersion forces includes both the Casimir and van der Waals forces between layered dielectrics.

Two conditions are required for the occurrence of a Casimir force: (i) a fluctuating field and (ii) a geometric restriction where the fluctuating field is required to satisfy certain conditions on the geometric boundary [4]. If a *critical system* is confined between two fixed boundaries then the long-range critical fluctuations near a continuous or second-order phase transition can generate an additional critical Casimir force between the boundaries which exists over and above the (noncritical) dispersion force. The fluctuating field in this case is given by the local order parameter. The existence of a Casimir force in a critical system confined between two dielectric plates was first predicted by Fisher and de Gennes (FdG) [5] using scaling theory. For a critical system of infinite size, the correlation length $\xi(T)$ is the only relevant length scale near the bulk critical temperature T_c; hence the leading order singular part of the critical free energy per unit area (ω_c) is governed by the power law

$$\frac{\omega_c}{k_B T_c} \sim \xi^{-(d-1)} \tag{1}$$

in d dimensions. Near T_c, the correlation length diverges as $\xi=\xi_0 t^{-\nu}$, where ν is a bulk critical exponent and the reduced temperature $t=|T-T_c|/T_c$. This implies that

$$\frac{\omega_c}{k_B T_c} \sim t^{+(d-1)\nu}. \tag{2}$$

However, all experimental systems are finite in size; hence other relevant macroscopic length scales may enter for finite-size systems. For example, if the experimental system resembles a uniform film, the film thickness L is a relevant length scale. According to the finite-size scaling ansatz of FdG, L will enter as the dimensionless combination L/ξ in the singular part of all thermodynamic functions. For such a system the power-law behavior of the singular part of the free energy [Eq. (2)] is replaced by the scaling law [6]

$$\frac{\omega_c}{k_B T_c} \sim t^{+(d-1)\nu} g^{ab}(L/\xi) \sim L^{-(d-1)} \theta^{ab}(L/\xi), \tag{3}$$

where $\theta^{ab}(y)=y^{-(d-1)}g^{ab}(y)$ is a universal finite-size scaling function; the superscript ab specifies the surface universality classes on the two confining boundaries of the film. At bulk criticality where $y=L/\xi=0$, $\theta^{ab}(0)=\Delta^{ab}$ defines a universal amplitude known as the Casimir amplitude [7]. The Casimir amplitudes Δ^{ab} characterize the contribution of the Casimir effect to the surface free energy at the bulk critical temperature T_c, whereas the universal finite-size scaling functions $\theta^{ab}(L/\xi)$ determine the temperature and size de-

pendence of the Casimir effect above and below T_c [8,9]. For $L \gg \xi$ bulk critical fluctuations will not be affected by the presence of the confining boundaries and any finite-size effects on the critical behavior will be negligible. However, when $t \to 0$ the correlation length can grow to infinity only in lateral directions. The system then becomes effectively two dimensional and therefore deviations from the bulk critical behavior are expected. These deviations are captured by the universal finite-size scaling functions and universal Casimir amplitudes.

Two approaches have been suggested for the experimental verification of Casimir effects in critical fluids having film geometries [7,10]. If both surfaces of the film are fixed then information about the finite-size scaling functions and the Casimir forces can be obtained by measuring the thickness of the film and the corresponding force between the surfaces. An atomic force microscope [11] or a surface forces apparatus [12] could be used for this purpose; both the separation distance and the force can be accurately and independently measured using these techniques. The second approach involves the study of equilibrium wetting films close to the critical point. In this case the determination of the Casimir force requires film thicknesses that are of the order of the correlation length. These can be obtained by partially immersing a molecularly smooth and chemically homogeneous substrate, for example, into liquid ^{4}He near its λ transition or into a critical binary liquid mixture near its demixing transition [13]. Above the liquid surface an adsorbed film of the liquid or liquid mixture forms on the substrate and coexists in thermodynamic equilibrium with the bulk liquid at the bottom of the container. The extent of the adsorption depends upon the strength of the intermolecular interactions between the substrate and the vapor molecules. Within the adsorbed film the solid substrate forms one of the boundary conditions while the free liquid/vapor surface forms the other boundary condition. Far away from T_c, the thickness of the film is primarily governed by the van der Waals force [14,15]. Near T_c the critical Casimir force between the film boundaries forms an additive contribution to the force balance equation for the film, which manifests itself in the equilibrium film thickness. Hence any experimental techniques that can accurately measure the adsorbed film thickness as a function of temperature near the bulk critical temperature can obtain information about the critical finite-size scaling functions $\theta^{ab}(L/\xi)$ and the universal Casimir amplitudes Δ^{ab}. In this paper we use the experimental technique of ellipsometry to conduct such a study of critical finite-size effects within a binary liquid film adsorbed onto a molecularly smooth and homogeneous silicon wafer. A general review of fluctuation-induced forces is provided in [4], while for more specific reviews aimed at Casimir forces induced by critical fluctuations see [7,10].

The plan of this paper is as follows. In Sec. II we review relevant theoretical considerations which determine the leading order singular part of the film surface free energy near criticality. In Sec. III the conditions that determine the equilibrium film thickness are specified. The experimental configuration, sample and substrate considerations, and the experimental technique of ellipsometry are described in Sec. IV. In Sec. V we report the experimental results and analyze them in the context of finite-size scaling. Our conclusions are provided in Sec. VI.

II. FINITE-SIZE SCALING FUNCTIONS AND AMPLITUDES

The forms of the scaling functions $\theta^{ab}(y)$ and the values for the Casimir amplitudes Δ^{ab} depend upon *both* the *system universality class* (i.e., Ising, *XY*, etc.) and the *boundary conditions* at each surface *a* and *b* [13,16,17]. These dependencies are expected. The critical finite-size behavior must return to bulk critical behavior determined by the system universality class in the limit as the film thickness $L \to \infty$. Additionally, the boundary conditions perturb the local order parameter (the local volume fraction in the case of a critical binary liquid mixture) within a distance ξ of the boundary, and this surface perturbation plays a significant role in influencing the critical finite-size behavior when the film thickness $L \sim \xi$ [5]. There are a number of differing boundary conditions that impose different *surface universality classes* on a system [18]. The surface may enhance the order in the vicinity of an interface so that the system undergoes a second-order phase transition in the presence of an *ordered* surface. This surface ordering can occur either spontaneously at a surface critical temperature $T_{cs} > T_c$ (designated the extraordinary transition *E*) or can be imposed by the presence of surface fields h_a and h_b at the two walls (normal transition *N*). Recently it has been demonstrated that the dominant critical behavior is identical for the extraordinary and normal transitions [19]. Other types of boundary condition can exist: the surface may suppress the order in the vicinity of an interface so that the system undergoes a second-order phase transition in the presence of a disordered surface (ordinary transition *O*); alternatively, both the surface and the bulk can simultaneously order at the same critical temperature (special transition SB).

In this publication we are most concerned with critical binary liquid mixtures in a confined film. It is well known that the bulk critical behavior for such systems is described by the Ising universality class corresponding to a scalar order parameter with two states, up or down for a magnetic system, or *A* or *B* for an *AB* critical binary liquid mixture [20]. In liquid mixtures the surface fields h_a and h_b are proportional to the more familiar surface tensions or surface free energies between the liquid and the confining boundary; the component (*A* or *B*) with the lowest surface free energy will preferentially adsorb against the boundary. This preferential adsorption is called critical adsorption in critical binary liquid mixtures and occurs at all noncritical surfaces [5,21], such as the container wall or a coexisting vapor phase (provided a wetting layer does not occur at this interface [22]). Critical adsorption influences the local volume fraction $v(z)$ of component *A* within a distance ξ of the surface. This is usually expressed using a local order parameter [23]

$$\psi^{ab}(z) = v(z) - v_c = M_- t^{\beta} Q_{\pm}(z/\xi_{\pm}, h_a t^{-\Delta_1}, h_b t^{-\Delta_1}, L/\xi_{\pm}), \tag{4}$$

where z is a measure of the distance from the wall at $z=0$ which possesses a surface field h_a. In this equation the second wall at $z=L$ possesses a surface field h_b, v_c is the

TABLE I. Theoretical results for the critical Casimir pressure.

d	Δ^{++}	Δ^{+-}	y_{peak}^{++}	y_{peak}^{+-}	ϑ_{max}^{++}	ϑ_{max}^{+-}	Ref.
2	−0.06545	1.505	2.23	−0.4821	−0.43	1.533	[16,27]
3	−0.428–0	0.279–3.1					[16,25,26]
4	−1.79	7.19	3.49	−5.28	−2.50	10.138	[25,26,28]

critical volume fraction of component A, $M_- t^\beta$ describes the shape of the bulk coexistence curve, $\xi_\pm = \xi_{0\pm} t^{-\nu}$ is the correlation length, β, ν, and Δ_1 are critical exponents, $Q_\pm$ is a universal function, and the subscript $+$ $(-)$ refers to a quantity in the one (two) -phase region of the liquid mixture. Sufficiently close to T_c the surface fields $h_a t^{-\Delta_1}, h_b t^{-\Delta_1} \to \pm\infty$ correspond to complete saturation of component A $(+\infty)$ or B $(-\infty)$ and $Q_\pm$ must lose its dependence upon the *specific* value of h_a or h_b; hence it is adequate under these circumstances to represent h_a or h_b by a $+$ or $-$ sign depending upon whether A or B prefers to adsorb against a surface. Our experimental technique is not sensitive to the local order parameter $\psi^{ab}(z)$ directly. Instead, our measurements are sensitive to the free energy per unit area ω_c [Eq. (3)] associated with the distortion in the composition profile as the two surfaces are brought within a distance of order $\sim\xi$ of each other. According to mean-field theory the distortion in the order parameter $\psi^{ab}(z)$ is related to ω_c via the equation [24]

$$\omega_c \sim \int \left(\frac{d\psi^{ab}(z)}{dz} \right)^2 dz. \tag{5}$$

For mean-field theory, Eqs. (4) and (5) reproduce the result in Eq. (3) where the surface fields h_a and h_b in Eq. (4) are represented by the sign $(+$ or $-)$ assigned to each of the superscripts a and b in the function $\theta^{ab}(y)$ in Eq. (3). There are only two different boundary conditions for ab that need to be considered: similar boundary conditions $(++)$, where the same component preferentially adsorbs at both surfaces, and opposite boundary conditions $(+-)$, where different components adsorb at the two surfaces.

The functional forms of $\theta^{ab}(y)$ and the values for Δ^{ab} have been determined theoretically for only a limited number of system universality classes possessing differing boundary conditions [13,16,17,25,26]. Thin film critical binary liquid mixtures are modeled using an Ising system possessing surface fields h_a and h_b at $z=0$ and L, respectively. For this case the universal scaling function $\theta^{ab}(y)$ has not been determined theoretically in the experimentally relevant dimension of $d=3$. However, the composition profile $\psi^{ab}(z)$ has recently been determined using a local functional theory [26] at criticality $(y=L/\xi=0)$; these results can probably be readily generalized to $y\neq 0$ and hence it seems that $\theta^{ab}(y)$ will be available in the near future. At present, estimates for the universal amplitudes Δ^{++} and Δ^{+-} are available from renormalization group theory [16], Monte Carlo calculations [25], and local functional theory [26]. There is a considerable variation in the values for these amplitudes; this variation is listed in Table I along with the exact values for these amplitudes in dimensions $d=2$ [16,27] and $d=4$ [25,26,28].

In the next section it will be found that the critical Casimir pressure (or critical Casimir force per unit area) determines the thickness of an adsorbed film near T_c. This critical Casimir pressure p_c is related to ω_c [Eq. (3)] by the equation [17]

$$p_c = -\frac{d\omega_c}{dL} = \frac{k_B T_c}{L^3} \vartheta^{ab}\left(\frac{L}{\xi_\pm} \right), \tag{6}$$

where the universal Casimir pressure scaling function ϑ^{ab} in Eq. (6) is related to the universal critical Casimir energy scaling function θ^{+-} in Eq. (3) via the expression

$$\vartheta^{ab}(y) = 2\theta^{ab}(y) - y\frac{d\theta^{ab}(y)}{dy}. \tag{7}$$

At criticality $\vartheta^{ab}(0) = 2\Delta^{ab}$. The universal scaling functions $\vartheta^{ab}(y)$ with $ab=++$ and $ab=+-$ have been calculated in dimensions 2 [23,29] and 4 [25]; they possess similar features. For the purposes of later comparison with experiment the mean-field expressions $(d=4)$ for $\vartheta^{++}(y)$ and $\vartheta^{+-}(y)$ obtained from [25] are plotted in Fig. 1; these mean-field results have been rescaled to provide agreement at T_c with the estimates of Δ^{++} and Δ^{+-} (Table I) that were calculated from renormalization group theory [25,26]. A number of generic features can be deduced from Fig. 1, which are also applicable for $d=2$, and are expected to be valid in $d=3$. (i) The functions $\vartheta^{++}(y)$ and $\vartheta^{+-}(y)$ are, respectively, nega-

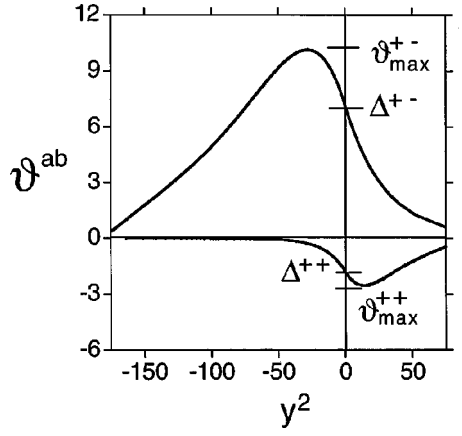

FIG. 1. Mean-field $(d=4)$ Casimir pressure scaling function $\vartheta^{ab}(y)$ as a function of the scaling variable $y^2=(L/\xi)^2$ for similar $(++)$ and opposite $(+-)$ boundary conditions within a critical thin film of thickness L. Here ξ is the correlation length and by convention $y^2>0$ represents the one-phase region while $y^2<0$ represents the two-phase region. These curves were obtained from [25] where the value at criticality $(y=0)$ has been rescaled by the universal Casimir amplitude Δ^{ab} obtained from renormalization group theory [25,26].

tive and positive for all y; we will later see (Sec. III) that the sign of $\vartheta^{ab}(y)$ determines whether critical fluctuations thin [$\vartheta^{ab}(y)$ negative] or thicken [$\vartheta^{ab}(y)$ positive] an adsorbed film. (ii) The functions $\vartheta^{++}(y)$ and $\vartheta^{+-}(y)$ exhibit a peak in, respectively, the one- and two-phase regions. This peak position occurs at y^{ab}_{peak} with a value ϑ^{ab}_{max}. We list y^{ab}_{peak} and ϑ^{ab}_{max} for $d=2$ [23,29] and 4 [25] in Table I. (iii) The absolute magnitude of $\vartheta^{+-}(y)$ is expected to be substantially larger than $\vartheta^{++}(y)$ in all dimensions; hence, critical finite-size effects should be easier to observe for asymmetric boundary conditions $(+-)$ than for symmetric boundary conditions $(++)$. In this publication we have therefore chosen to study films possessing asymmetric boundary conditions where critical finite-size effects are expected to be largest.

Evidence for critical finite-size effects in thin adsorbed films of a Lennard-Jones binary fluid mixture have recently been obtained in a Monte Carlo simulation [30]; however, in this study it was difficult to definitively understand the Casimir forces because of long computational equilibration times and limitations on the system size that could be studied. Critical finite-size effects have also recently been observed in thin films of ^{4}He near the superfluid transition T_λ [31]. This system is believed to belong to the XY universality class with OO boundary conditions [13,16,17]. The universal scaling function $\theta^{OO}(y)$ and universal amplitude Δ^{OO} for this system are expected to be rather different from those studied here. In this case $\Delta^{OO}(\sim -0.022)$ is much smaller and of opposite sign to $\Delta^{+-}(\sim 0.29$ to $3.1)$. Consequently, critical finite-size effects will thin an adsorbed ^{4}He film; the magnitude of this thinning is predicted to be considerably smaller than the thickening expected in critical liquid mixture films because $|\Delta^{OO}| \ll \Delta^{+-}$. Garcia and Chan [31] find reasonable agreement with theoretical expectations that are available for $T \geqslant T_\lambda$ [13,17].

III. SURFACE FREE ENERGY CONSIDERATIONS

In Fig. 2 we depict schematically the generic situation that is of most interest to us, namely, an adsorbed film on a solid substrate which is suspended horizontally or vertically above the liquid/vapor surface of a critical binary liquid mixture. The adsorbed film for $+-$ boundary conditions is expected to possess a composition near the bulk critical composition of the liquid mixture, at least for $T > T_c$ [25,32]. This film forms on the solid substrate via the interactions between the substrate and the vapor molecules. We study the adsorbed film thickness L as a function of height H above the liquid/vapor surface and as a function of reduced temperature t from the bulk critical temperature T_c. Various elements come into play in determining the thickness of this adsorbed film. We will assume that both surfaces of the film are sharp and that capillary wavelike fluctuations at the film's liquid-vapor surface are small. The equilibrium film thickness L is determined by minimizing the free energy per unit area of this liquid layer, which in the limit of large interfacial area A can be written in the form [17]

$$\lim_{A\to\infty} \frac{\mathcal{F}(T,L)}{A} = \sigma_{sl}(T) + \sigma_{lv}(T) + w_{nc}(T,L) + w_c(t,L), \tag{8}$$

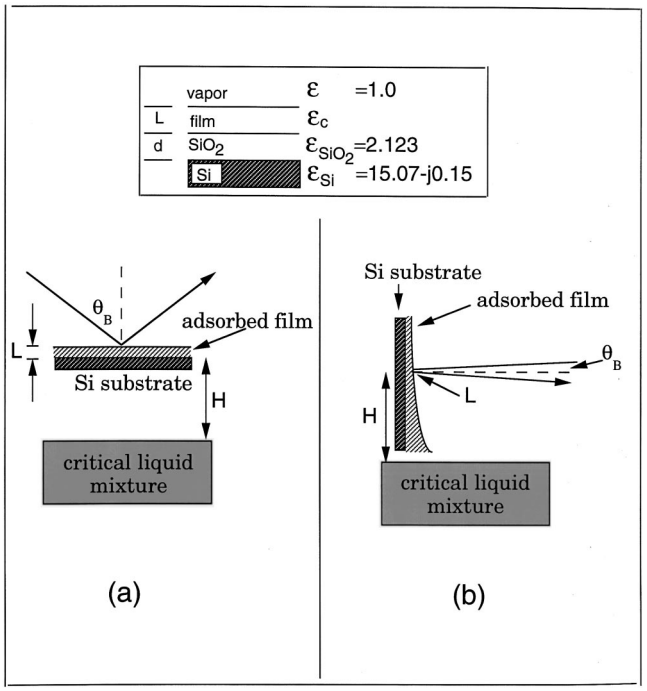

FIG. 2. Schematic diagram showing the (a) horizontal and (b) vertical substrate geometry. The inset depicts the dielectric model used to obtain the adsorption film thickness L for films on an oxide coated Si wafer.

where σ_{ij} represents the surface energy between phases i and j with $s \equiv$ substrate, $l \equiv$ liquid, and $v \equiv$ vapor, w_c [Eq. (3)] is the contribution from critical fluctuations, while w_{nc} is a noncritical contribution that is present at all temperatures and will be described in more detail below. Each of the contributions σ_{sl}, σ_{lv}, and w_{nc} depends only weakly on the absolute temperature T in an analytic and nonsingular way and therefore over the small temperature range that we consider their temperature dependence can be neglected; in contrast, w_c depends strongly on T especially in the vicinity of T_c. Sufficiently far from T_c, however, $w_c \sim \exp(-L/\xi)$ and this term will be negligible compared with the other terms in Eq. (8) provided $L/\xi \gg 1$.

Let us now consider the various contributions to the noncritical term w_{nc}. At a height H above the liquid/vapor surface the vapor pressure p is a function of H and molecules at this height possess an additional gravitational potential energy per unit area w_g, relative to molecules immediate above the liquid/vapor surface at saturated vapor pressure p_{sat}, where

$$w_g = -\frac{k_B T L}{V} \ln(p/p_{sat}) = \rho g H L \tag{9}$$

and V is the volume per molecule. At height H the vapor is also in equilibrium with the adsorbed film on the substrate, which provides the second equality in Eq. (9) [15] where $\rho = \rho_l - \rho_v \approx \rho_l$ is the density difference between the liquid film (l) and the vapor (v) and g is the acceleration due to gravity. For all substrate surfaces there is a long-range van der Waals interaction per unit area between the substrate and

the vapor phase, which for sufficiently thin films ($L \lesssim 10$–20 nm), in the nonretarded regime, takes the form [15]

$$w_{vdw}(T,L) = \frac{W(T)}{L^2}, \tag{10}$$

where $W(T)$ is the well-known Hamaker constant which depends upon the polarizabilities of the bulk phases. (Note that our definition for $W = -W_I/12\pi$ where W_I is the Hamaker constant defined by Israelachvili [15].) A more accurate but necessarily more complicated description of w_{vdw} is provided by the DLP theory for dispersion interactions [3] and includes the nonadditivity of the intermolecular interactions as well as retardation effects. In this theory w_{vdw} is expressed in terms of the frequency-dependent dielectric properties of the bulk phases [33,34]. For film thicknesses that are of the order of a few times the molecular diameter, the continuum theory for the van der Waals interaction breaks down and oscillatory solvation interactions within the adsorbed film (determined by packing of the liquid molecules against the hard substrate wall) become important. To account for this we must include a monotonic repulsive structural interaction [35]

$$w_{struct}(T,L) = -A \exp(-L/\delta), \tag{11}$$

where δ is of order a molecular diameter. The total noncritical contribution to the film surface free energy that appears in Eq. (8) is therefore

$$w_{nc} = w_g + w_{vdw} + w_{struct}. \tag{12}$$

At a particular height H and reduced temperature t the *equilibrium thickness* of the adsorbed film is determined by that value of L which minimizes $\mathcal{F}/A$ [Eq. (8)], namely,

$$\left(\frac{d(\mathcal{F}/A)}{dL}\right) = 0 \tag{13}$$

at equilibrium. This minimization gives

$$\vartheta^{+-}\left(\frac{L}{\xi_\pm}\right) = \frac{1}{k_B T_c}\left(-2W + \rho g H L^3 + \frac{AL^3}{\delta}\exp(-L/\delta)\right), \tag{14}$$

where $\vartheta^{+-}(y)$ is the universal Casimir pressure scaling function introduced in Eq. (6).

Equation (14) is the principal equation that controls the thickness of the adsorbed film. It exhibits various limiting forms, which have been observed under differing conditions. For example, sufficiently far from T_c when $\vartheta^{+-}(L/\xi_\pm) \sim \exp(-L/\xi_\pm) \approx 0$ (provided $L/\xi_\pm \gg 1$) Eq. (14) reduces to

$$\frac{-2W}{L^3} + \rho g H + \frac{A}{\delta}\exp(-L/\delta) = 0. \tag{15}$$

Later in this paper (Sec. V) this equation will be used to determine the system-dependent parameters W, A, and δ by studying the film thickness L as a function of height H at fixed $T \gg T_c$. For $L \gg \delta$ the structural contribution is negligible and Eq. (15) leads to the well known relationship [14]

$$-2W + \rho g H L^3 \approx \vartheta^{+-} \approx 0, \tag{16}$$

which is valid for thin film thicknesses L in the nonretarded regime. For thicker films the full DLP theory of dispersion interactions must be used [3]; the full theory has been verified for adsorbed films under somewhat different circumstances from those considered here [36]. Equation (16) indicates another essential requirement for an adsorbed film to exist far from T_c, specifically, $W > 0$ which for our situation (Fig. 2) normally implies that the optical dielectric constant $\varepsilon(\text{substrate}) > \varepsilon(\text{film})$ [22].

How does the critical contribution $\vartheta^{+-}(L/\xi_\pm)$ in Eq. (14) influence the behavior of the film near T_c? To answer this question it is easiest to consider the simplified version given in Eq. (16) where the structural forces have been neglected. For $T \gg T_c$ where $\vartheta^{+-}(L/\xi_\pm) \approx 0$ the film thickness is determined by Eq. (16); however, as T is slowly decreased toward T_c so that ϑ^{+-} is no longer zero, it is easy to see from Eq. (16) that the film thickness L increases (decreases) if ϑ^{+-} is positive (negative). From the theoretical results discussed in Sec. II $\vartheta^{+-}(y)$ is expected to be positive for all y; hence the adsorbed film should thicken as T_c is approached within the one-phase region. Additionally, according to Fig. 1 and Table I the thickness is expected to attain a maximum value in the two-phase region. In Sec. V, once the system-dependent parameters W, A, and δ have been determined at $T \gg T_c$ using Eq. (15), scaling can be checked and the function $\vartheta^{+-}(L/\xi_\pm)$ deduced by studying the L dependence as a function of t at fixed H using Eq. (14).

IV. EXPERIMENTAL DESIGN

From our earlier discussion (Sec. II) we have chosen to study critical finite-size Casimir effects in adsorbed critical binary liquid mixture films possessing opposite boundary conditions $(+-)$, where the effects are expected to be large. The substrate on which the film adsorbs should be molecularly smooth in order to simplify the experimental interpretation of the film thickness and also minimize complications from adsorption on rough surfaces. We have therefore chosen to study vapor adsorption on a molecularly smooth [100] Si wafer. These wafers were purchased from Semiconductor Processing Company. They are polished on one side, exhibit a surface roughness of ~ 0.5 nm measured using an atomic force microscope in contact mode, possess *n*-type phosphorus doping, and have a resistivity of 1–10 Ω cm. The wafers are 3 mm thick, which ensures that they are flat over macroscopic distances ($\sim$cm). The wafers were diamond sawed to the required length and width for our sample cell after first protecting the polished side using a strong plastic adhesive tape. Any residual adhesive or organic or metallic impurities were then removed using the following standard silicon wafer cleaning procedure [37]. The wafer was first immersed in an ultrasonic bath of pure acetone for 10 min to remove gross contaminants. Organic contaminants were then removed using a solution of $H_2O + H_2O_2 + NH_4OH$ in the ratio 6:1.5:1 for 15 min at 75 °C. This was followed by a solution consisting of $H_2O + H_2O_2 + HCl$ in the ratio 7.5:1.5:1 for 15 min at 75 °C to remove metallic contaminants. The wafer was finally rinsed in distilled deionized water and then vapor degreased in isopropyl alcohol [38].

Isopropyl alcohol and water are completely miscible so that any residual water on the wafer surface is removed and the substrate can be readily dried in an oven at 110 °C without leaving any observable ''water stains.'' Just prior to use the wafers were uv ozone cleaned [39] for one hour to remove any trace organic contaminants. This cleaning procedure leaves the Si wafer surface hydrophilic with a thin passive oxide layer.

Our initial experiments studied adsorption on a horizontal Si wafer cut to fit inside a clean, glass-etched [40], cylindrical pyrex sample cell of diameter ~ 2.5 cm and length ~ 8 cm. This sample cell was placed inside a two-stage oven possessing a thermal stability of ~ 1 mK over 4 h, where the oven was carefully designed to minimize the presence of any thermal gradients. The critical liquid mixture rested at the bottom of the sample cell at a fixed height H below the polished surface of the Si wafer [Fig. 2(a)]. The horizontal geometry for the Si wafer did not prove to be ideal because (i) it was difficult to ensure that the Si wafer was precisely horizontal, (ii) the height H could only approximately be estimated, and (iii) it was difficult to independently determine the background term ω_{nc} [Eq. (12)] for this configuration (Sec. V). The adsorbed film thickness on the horizontal Si wafer was measured as a function of temperature using a phase-modulated ellipsometer [41] which possessed a *vertical* plane of incidence.

In later experiments, which provided more definitive experimental results, a new phase-modulated ellipsometer was built. It possesses a *horizontal* plane of incidence. The Si wafer is now suspended vertically above a critical binary liquid mixture [Fig. 2(b)] inside a cylindrical glass cell where a metal clip mechanically holds the wafer against a chemically resistant stainless-steel plate (type 316). The glass cell possesses a threaded neck (Ace Glass, Cat. No. 7644) so that positive pressure applied to a Teflon bushing (Ace Glass, Cat. No. 7506) compresses a Teflon coated O ring between the stainless-steel plate and the glass cell wall (Fig. 3), thus sealing the cell. A Teflon coated magnetic stirrer bar rests at the bottom of the sample cell in the liquid mixture. The mixture can readily be mixed using a magnetic stirrer motor external to the two-stage thermostat in which the sample cell is positioned. A He-Ne laser beam from the ellipsometer, which is focused to a small spot (~ 0.25 mm), is reflected off the Si wafer surface at a height H above the liquid/vapor surface at an angle of incidence equal to the Brewster angle θ_B. The signal measured by the ellipsometer ($\overline{\rho}$) is very sensitive to surface structure at this angle of incidence [42] and can be readily interpreted in terms of a film thickness. The thermostat is attached to a translation stage which can move up and down in a vertical plane driven by a dc stepping motor controller with a resolution of 10 μm. Hence measurements of the film thickness on the Si wafer can be taken at any vertical position along the wafer. The temperature of the sample cell is controlled by a two-stage thermostat, constructed from concentric metallic shells that are thermally isolated from each other. The inner shell consists of symmetrically wound heater wires whose temperature is regulated by a commercial temperature controller, while the outer water-cooled shell, at constant temperature, acts as a heat sink. These two stages possess a combined thermal stability of ~ 0.1 mK over two hours and

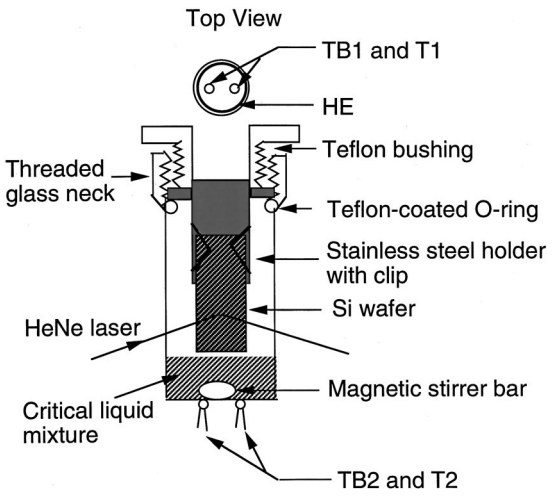

FIG. 3. Illustration of the construction of the sample cell for the vertical Si wafer. T1 and T2 are matched precision thermistors to measure the temperature at either end of the sample cell while TB1 and TB2 are matched precision thermistors used in an ac bridge circuit that is used to minimize the presence of any thermal gradients along the length of the sample cell by supplying current to the heater HE.

~ 1 mK over a day, as measured by two matched precision thermistors (Yellow Springs Instruments, Cat. No. 44034) placed at either end of the sample cell (T1 and T2, Fig. 3). Unfortunately, a temperature gradient of ~ 5 mK/cm was present along the length of the sample cell, which can cause serious problems in the measurement of adsorbed films. We have used an ac bridge technique to minimize this thermal gradient along the sample cell. One-half of the bridge is formed by two matched precision thermistors at either end of the sample cell (TB1 and TB2, Fig. 3) while the other half of the bridge is formed by a seven-decade precision ratio transformer (Electro Scientific Industries, Model 73). The bridge imbalance is amplified by a preamplifier and converted to a dc error signal using a lock-in amplifier. The output of the lock-in amplifier is amplified, integrated, differentiated, and then summed; the resulting signal provides the feedback that controls the current supplied to a heating element situated in the upper end of the stainless-steel holder (HE, Fig. 3). Using this technique, temperature gradients can be reduced to less than 50 μK/cm along the length of the sample cell. Within each of the metal shells of the thermostat, vertical apertures allow the passage of a laser beam for incident angles between 65° and 77°, in the vicinity of the Brewster angle for a bare Si wafer. To minimize heat loss caused by convection, annealed glass windows cover these apertures. The glass windows and the cylindrical sample cell can shift the angle of incidence for the laser beam by a few tenths of a degree away from the calculated Brewster angle for the Si wafer; however, minor shifts in the angle of incidence near the Brewster angle do not cause serious problems for the ellipsometric technique because the ellipticity $\overline{\rho}$ is relatively insensitive to the angle of incidence in this region [43]. Window covered ports within the thermostat also allow passage of a laser beam through the bulk critical liquid mixture so that the critical temperature of the mixture can be determined *in situ* with an accuracy of ~ 1–2 mK by observing the

TABLE II. Critical liquid mixture properties $V(H) \equiv$ vertical (horizontal) Si wafer geometry.

	T_c (K)	m_c[a]	ϵ_c[b]	ξ_{0+}[c] (nm)	$10^{24}W$ (J)	δ (nm)	A (J/m^2)	L^* (nm)	$10^{21}W_{DLP}$ (J)	Φ[d]
MH	306.83 (V)	0.673	1.846	0.30	1.19 (V)	0.50	3.3×10^{-5}	3.60	0.9	22°
	307.10 (H)				2.90 (H)					
MM	298.05 (V)	0.566	1.994	0.37	0.68 (V)	0.15	4.2×10^{2}	3.82		38°
	299.80 (H)				0.45 (H)					

[a]Critical mass fraction of hexane (methylcyclohexane) for MH (MM).
[b]Optical dielectric constant at the critical composition for these two mixtures.
[c]Correlation length amplitude in the one-phase region determined from critical adsorption measurements as described in [50].
[d]Contact angle at temperature $T=333$ K (346 K) for MH (MM).

spinodal ring generated during the process of spinodal decomposition.

The vertical Si wafer configuration is far more versatile than the horizontal Si wafer configuration because for the vertical wafer H can be measured accurately and varied continuously; from a study of the adsorption thickness L as a function of height H the system-dependent parameters W, A, and δ can be determined using Eq. (15) at fixed $T \gg T_c$. It is difficult to deduce these parameters experimentally for the horizontal Si wafer. In the vertical geometry it is important to suspend the Si wafer *above* the liquid mixture during the measurement of the adsorption film thickness. If the Si wafer is dipped into the liquid mixture, very long lived thick metastable films have been observed on the Si wafer. These films are created during changes in temperature; differences in the thermal capacities and thermal conductivities of components within the sample cell create large temperature gradients between the bulk liquid mixture and the top of the Si wafer. These thermal gradients generate thermocapillary flow and (macroscopic) ''phase separation'' on the Si wafer due to the differences in surface tension between the two liquid components. This ''phase separation'' is observed as a very thick film at the base of the Si wafer as deduced by the presence of interference fringes which persist for many days even after thermal equilibrium has been reached and the thermal gradients have disappeared. Hence, from an experimental point of view, it is much more efficient to suspend the Si wafer above the liquid mixture so that the films form by adsorption from the vapor and there is no perturbing influence due to thermocapillary driven flow up the meniscus.

In this paper we study two critical systems, methanol + hexane (MH) and 2-methoxyethanol + methylcyclohexane (MM) [44], which form adsorbed films belonging to the $+-$ surface universality class on the Si wafer. Here one boundary of the film is the silicon wafer while the other boundary is the free liquid-vapor surface. The component with the lower surface tension preferentially adsorbs at the liquid-vapor surface while the boundary condition at the Si wafer surface can be determined by examining whether the liquid-liquid meniscus bends up or down against the wafer in the two-phase region of the liquid mixture. For MH (MM) at the liquid-vapor surface hexane (methylcyclohexane) adsorbs at this surface while methanol (2-methoxyethanol) adsorbs at the liquid-substrate surface. These two mixtures therefore constitute an experimental realization of the $+-$ boundary condition. Experimental parameters relevant to each mixture are provided in Table II.

The film thickness measurements were performed using phase-modulated ellipsometry, which is a technique that detects changes in the state of polarization for light reflected from a surface [45]. If $r_{s(p)}$ denotes the complex reflection amplitude of the light for polarization $\perp(\parallel)$ to the plane of incidence, then the ellipticity $\overline{\rho}=\mathrm{Im}(r_p/r_s)|_{\theta_B}$ at the Brewster angle θ_B defined by $\mathrm{Re}(r_p/r_s)|_{\theta_B}=0$ is very sensitive to surface structure. In the absence of any capillary wave fluctuations $\overline{\rho}$ is related to the optical dielectric profile $\epsilon(z)$ at depth z within the interface by the Drude equation [46]

$$\overline{\rho}=\frac{\pi}{\lambda}\frac{\sqrt{\epsilon_1+\epsilon_3}}{\epsilon_1-\epsilon_3}\int\frac{[\epsilon(z)-\epsilon_1][\epsilon(z)-\epsilon_3]}{\epsilon(z)}dz, \qquad (17)$$

where ϵ_1 and ϵ_3 represent the optical dielectric constants of the incident ($z\to-\infty$) and the substrate media ($z\to\infty$), respectively. This formula assumes that $\epsilon(z)$ is locally isotropic and that the thickness of the film is small compared with the wavelength of light $\lambda=632.8$ nm.

A model for $\epsilon(z)$ is required in order to determine the adsorption film thickness L from ellipsometric data. This can be obtained using the Clausius-Mossotti relation applicable to a mixture [47],

$$F(\epsilon(z))=v(z)F(\epsilon_A)+[1-v(z)]F(\epsilon_B), \qquad (18)$$

where $v(z)$ is the volume fraction of component A at z, the function $F(x)=(x-1)/(x+2)$, and ϵ_i $(i=A,B)$ is the optical dielectric constant for component i. In Eq. (18) it is assumed that there is no volume change on mixing the two components. For our situation, a good approximation is to assume that $v(z)=v_c$ (the critical composition of A) so that $\epsilon(z)=\epsilon_c$ where ϵ_c is the dielectric constant of the bulk critical liquid mixture (Table II). This approximation is valid because all organic liquids possess similar optical dielectric constants $(\epsilon_A\approx\epsilon_B\sim2)$ and additionally $\epsilon_A,\epsilon_B\ll\epsilon_{\mathrm{Si}}=15.07-j0.15$, the optical dielectric constant for Si; hence within the adsorbed film there is little optical contrast between the two organic components and the film dielectric constant can be treated as a constant independent of z. Silicon wafers also normally possess a thin oxide layer of thickness d ($\sim$nm) and optical dielectric constant $\epsilon_{\mathrm{SiO_2}}$ $(=2.123)$; therefore a reasonable model for the adsorbed film on a Si wafer is the two-layer model exhibited in Fig. 2

(inset). With this model for $d, L \ll \lambda$ from Eqs. (17) and (18) $\bar{\rho}$ is proportional to the film thickness L,

$$\bar{\rho} = \frac{\pi}{\lambda} \frac{\sqrt{1+\epsilon_{\mathrm{Si}}}}{1-\epsilon_{\mathrm{Si}}} \left(\frac{(\epsilon_c - 1)(\epsilon_c - \epsilon_{\mathrm{Si}})}{\epsilon_c} L + \frac{(\epsilon_{\mathrm{SiO_2}} - 1)(\epsilon_{\mathrm{SiO_2}} - \epsilon_{\mathrm{Si}})}{\epsilon_{\mathrm{SiO_2}}} d \right). \quad (19)$$

Thicker films ($L + d \gtrsim 20$ nm) exhibit significant deviations from this linearity in L [45]; Maxwell's equations must then be solved numerically for the $p(r_p)$ and s wave (r_s) complex reflection amplitudes in order to interpret the ellipsometric data [48].

Our bare Si wafer surfaces typically gave $\bar{\rho} = 0.020 \pm 0.001$, which from Eq. (19) corresponds to an oxide film thickness of ~ 2.0 nm. The large real component for the Si dielectric constant provides a strong dependence for the ellipticity $\bar{\rho}$ upon the film thickness L. We measure $\bar{\rho}$ with a sensitivity of $\sim 10^{-5}$ corresponding to a thickness sensitivity of ~ 0.001 nm averaged over the size of the incident beam spot for organic liquids on silicon. All of our measurements were taken at a fixed angle of incidence close to the Brewster angle for the bare silicon wafer, $\theta_B = \tan^{-1}(n_3/n_1) = 75.53°$. In general, rather than using Eq. (19) to interpret the data (which assumes thin adsorbed films), we have used a matrix technique to numerically solve Maxwell's equations [48] for the configuration shown in Fig. 2 (inset), which enables $\bar{\rho}$ to be converted directly into film thickness L.

In a typical ellipsometric measurement the temperature is set and approximately 6 h is allowed for the system to attain thermal and diffusive equilibrium. Twenty $\bar{\rho}$ and T measurements are then collected over the succeeding 2 h. From these 20 measurements the mean and standard deviation for $\bar{\rho}$ are determined. For both critical liquid mixtures a typical standard deviation for each data set of 20 $\bar{\rho}$ measurements was $\sim 3 \times 10^{-4}$; however, different temperature scans on the same liquid mixture exhibited a reproducibility for $\bar{\rho}$ of $\pm 3 \times 10^{-3}$. We therefore took this latter value (corresponding to an error in L of ± 0.3 nm) as a conservative estimate for the error in $\bar{\rho}$.

V. EXPERIMENTAL RESULTS AND DISCUSSION

In Fig. 4 we show the adsorption thickness L as a function of temperature T collected from a horizontal Si wafer for both critical liquid mixtures MH (circles) and MM (crossed diamonds), where for clarity the MM data have been shifted vertically by 5 nm. The behavior is completely reproducible for both increasing and decreasing temperatures. Sufficiently far from the critical temperature T_c critical finite-size effects will be negligible; however, on approaching T_c the critical Casimir pressure scaling function $\vartheta^{+-}(L/\xi_{\pm})$ will play an increasingly important role in determining the thickness of the adsorbed film. As discussed in Sec. III, the increase in L in the vicinity of T_c and the peak in the two-phase region necessarily indicate that both Δ^{+-} and $\vartheta^{+-}(y)$ are positive and that $\vartheta^{+-}(y)$ possesses a peak in the two-phase region. All of these features are in qualitative agreement with theory

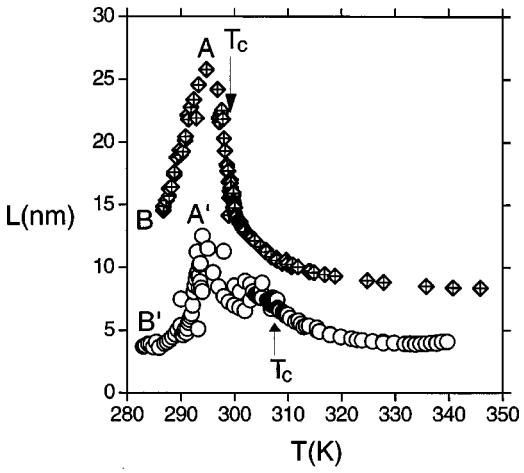

FIG. 4. Variation in the adsorption film thickness L as a function of temperature near the critical temperature T_c for the mixtures MH (circles) and MM (crossed diamonds) on a horizontal Si wafer where the height $H \approx 10$ mm. For clarity the MM data have been shifted vertically by 5 nm. A and A' label the peak positions in the two-phase region while B and B' label the data at the lowest temperature measured.

(see Fig. 1 and Table I). We note with caution, however, that the interpretation of the two-phase region is rather complicated; we therefore analyze the single-phase region in detail first. A preliminary account of the behavior of $\vartheta^{+-}(y)$ in the one-phase region has been given in [49]. As noted previously [49], the increase in the adsorption thickness L near T_c (Fig. 4) cannot be explained by any unusual behavior exhibited by either of the pure components of the binary liquid mixture.

For a quantitative analysis of the experimental data the system-dependent parameters W, A, δ, and $\xi_{0\pm}$ must be determined. The correlation length amplitude ξ_{0+} in the one-phase region has been determined using critical adsorption ellipsometric data following the procedure in [50]. The values for this amplitude for each liquid mixture are listed in Table II. It is difficult to determine the parameters W, A, and δ from measurements on the horizontal Si wafer. However, these parameters can be determined by examining the variation of the adsorption thickness L with height H on the vertical Si wafer for fixed $T \gg T_c$. In Fig. 5 we show L versus H for both systems at temperatures of 333 K for MH and 346 K for MM. Both temperatures are $\gtrsim 30\,°\mathrm{C}$ above T_c (Table II) for each system, where critical finite-size effects are expected to be small. In this region the thickness L does not change significantly with temperature T for fixed H (Fig. 4), as might be expected. Hence $\vartheta^{+-}(y)$ can be neglected and the data in Fig. 5 can be analyzed using Eq. (15). For sufficiently large L the structural contribution is negligible $(L/\delta \gg 1)$ and $L \sim H^{-1/3}$ [Eq. (16) and Fig. 5 (inset)] from which the Hamaker constant W can be determined (Table II). At sufficiently large H the adsorption thickness L loses its dependence upon H, i.e., L approaches a constant value L^*, which implies that the gravitational term $\rho g H$ in Eq. (15) does not play a major role in determining L^* and this thickness is instead determined by a competition between the dispersion interaction and the structural term. The parameter A can be expressed in terms of W, δ, and L^*,

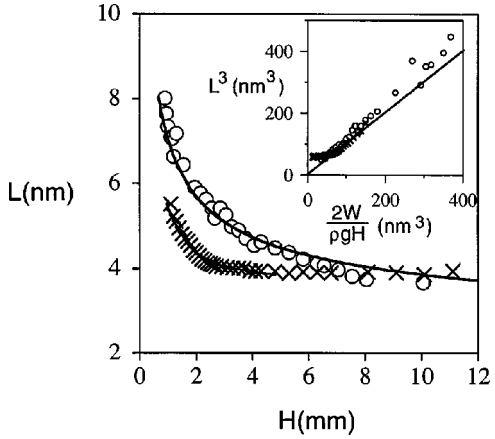

FIG. 5. Film thickness L as a function of height H for MH (circles) and MM (crosses) at temperatures of $T=333$ and 346 K, respectively. The solid lines are fits to Eq. (15) used in determining A and δ as described in the text. The inset illustrates the $L \sim H^{-1/3}$ dependence for small H (or large L) from which the effective Hamaker constant W is determined. The solid line in the inset has a slope of 1.

$$A=\frac{2W\delta}{L^{\star 3}}\exp(L^{\star}/\delta); \tag{20}$$

hence, if this expression is substituted into Eq. (15), only the parameter δ is undetermined. δ is adjusted to provide the best description of the crossover from $L\sim H^{-1/3}$ to $L=L^*$ behavior in Fig. 5 (solid lines). The parameters A, δ, and L^* are listed in Table II for both systems. As expected, δ is of order a molecular diameter [35]; however, the values determined for A for each system are quite different from each other and appear to be anomalously large or anomalously small compared with values determined by other methods, where $A\sim 1$ mJ/m^2 [35]. We attribute these anomalous A values to an imperfect understanding of the structural contributions that occur in our system, so that our representation of this term in Eq. (15) forms only an approximation for the correct behavior. The form for the structural term, which is

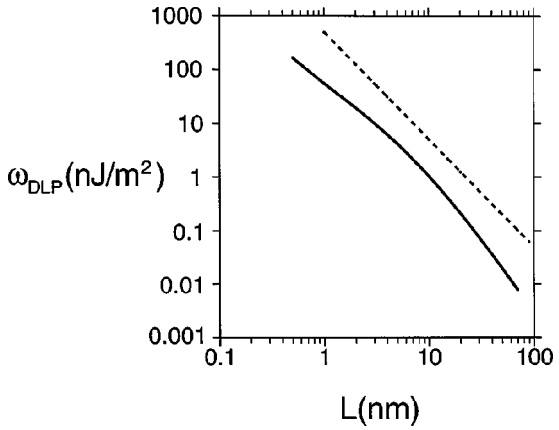

FIG. 6. Plot of the DLP dispersion free energy per unit area ω_{DLP} [51] for the mixture MH as a function of film thickness L. The dashed line illustrates the dependence $\omega_{DLP}\sim W_{DLP}/L^2$ for nonretarded interactions from which the DLP Hamaker constant W_{DLP} can be obtained.

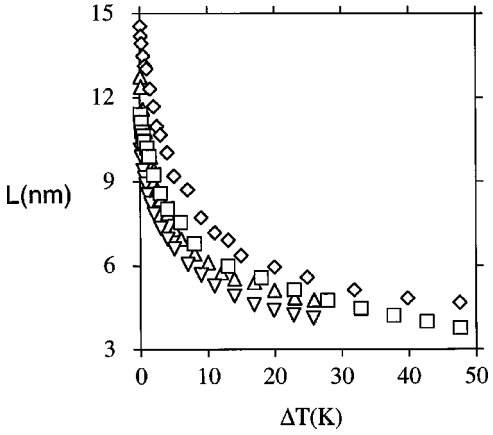

FIG. 7. Film thickness L as a function of $\Delta T=T-T_c$ at fixed heights $H=1.5$ mm (diamonds) and 3.3 mm (squares) for MM, and 3.4 mm (triangles) and 6.3 mm (inverted triangles) for MH, adsorbed on a vertical Si wafer.

determined by local interactions, is less well understood theoretically than any of the other terms that appear in Eq. (14). Later in this section (Fig. 8, inset) we will observe that the structural term has very little influence on the form determined for the universal scaling function $\vartheta^{+-}(L/\xi_{\pm})$; it plays an important role only for very thin noncritical films far from T_c. Therefore, for our purposes, the form of the structural term that we have assumed is adequate.

The values for the Hamaker constant W (Table II) are two to three orders of magnitude smaller than expected [15]. In Fig. 6 we show a theoretical calculation of the dispersion free energy per unit area ω_{DLP} as a function of the film thickness L from the DLP theory [3] for the system MH. This calculation determines the interaction energy per unit area between the bulk Si and air phases assuming a two-layer system consisting of a homogeneous film of thickness L at

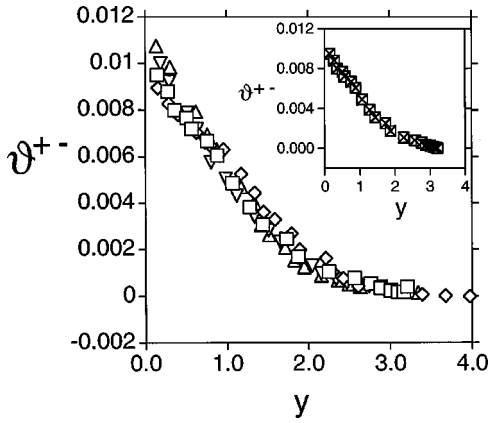

FIG. 8. The Casimir pressure scaling function $\vartheta^{+-}(y)$ obtained from a vertical Si wafer in the one-phase region for the two mixtures MH and MM. This graph was deduced by substituting the data in Fig. 7 into Eq. (14). The symbols have the same meaning as in Fig. 7. The function $\vartheta^{+-}(y)$ exhibits excellent scaling as a function of $y=L/\xi_+$ where L is the film thickness and ξ_+ is the correlation length in the one-phase region. In the inset we demonstrate that the structural contribution in Eq. (14) has a negligible influence on the shape of ϑ^{+-}. For MM at a height of $H=3.3$ mm the structural amplitude $A=0$ (crosses) or 420 J/m^2 (squares).

TABLE III. One-phase data.

$T(K)$	$\overline{\rho}\times10^3$	L(nm)	$y=L/\xi_+$	ϑ^{+-}	$T(K)$	$\overline{\rho}\times10^3$	L(nm)	$y=L/\xi_+$	ϑ^{+-}
	(a) MH, $H=6.3$ nm					(c) MM, $H=3.3$ mm			
332.593	35.0	4.12	2.88	0.0001	345.675	34.3	3.77	3.21	0.0000
329.643	36.0	4.24	2.75	0.0002	340.715	36.3	3.99	3.17	0.0001
326.703	37.4	4.40	2.61	0.0003	335.794	38.3	4.21	3.09	0.0002
323.746	39.1	4.60	2.47	0.0004	330.909	40.6	4.46	3.01	0.0003
320.789	41.8	4.92	2.34	0.0006	325.915	43.2	4.75	2.88	0.0004
317.808	44.9	5.28	2.16	0.0009	320.970	46.8	5.14	2.76	0.0006
315.826	48.3	5.68	2.05	0.0013	316.019	50.7	5.57	2.57	0.0008
313.862	51.4	6.05	1.87	0.0017	311.071	54.5	5.99	2.25	0.0011
311.867	56.1	6.60	1.65	0.0024	306.043	61.7	6.78	1.87	0.0017
310.863	59.1	6.95	1.51	0.0029	304.028	68.6	7.54	1.74	0.0025
309.869	62.4	7.34	1.34	0.0035	302.066	73.1	8.03	1.44	0.0031
308.894	66.7	7.85	1.12	0.0043	301.058	78.1	8.58	1.28	0.0039
308.395	69.9	8.22	0.99	0.0051	300.050	84.1	9.24	1.07	0.0049
307.900	72.6	8.55	0.81	0.0058	299.375	90.0	9.89	0.88	0.0061
307.680	75.8	8.91	0.73	0.0066	299.042	92.8	10.20	0.76	0.0067
307.480	77.7	9.14	0.63	0.0072	298.651	95.0	10.44	0.57	0.0072
307.280	79.9	9.40	0.51	0.0079	298.537	96.9	10.65	0.51	0.0077
307.000	84.0	9.88	0.29	0.0092	298.325	98.2	10.79	0.36	0.0080
306.910	86.1	10.13	0.19	0.0100	298.221	101.3	11.13	0.27	0.0088
	(b) MH, $H=3.4$ mm				298.110	103.8	11.41	0.14	0.0095
332.696	40.5	4.76	3.34	0.0000		(d) MM, $H=1.5$ mm			
329.772	41.1	4.84	3.15	0.0001	345.636	42.5	4.67	3.97	0.0000
326.787	43.4	5.11	3.05	0.0002	337.855	44.0	4.84	3.68	0.0000
323.796	45.8	5.39	2.90	0.0003	329.905	46.7	5.13	3.39	0.0001
320.804	47.0	5.53	2.63	0.0004	322.905	50.8	5.58	3.15	0.0002
318.872	48.8	5.74	2.49	0.0005	318.016	54.2	5.95	2.93	0.0003
316.881	51.9	6.11	2.36	0.0007	313.004	57.9	6.36	2.61	0.0004
314.872	54.6	6.42	2.16	0.0009	311.085	62.9	6.91	2.60	0.0007
312.876	59.0	6.94	1.95	0.0013	309.074	65.3	7.17	2.43	0.0008
311.876	62.0	7.29	1.83	0.0016	307.062	70.2	7.71	2.30	0.0011
310.872	66.9	7.87	1.71	0.0021	305.056	79.2	8.71	2.22	0.0017
309.863	71.1	8.36	1.52	0.0026	303.059	83.7	9.20	1.89	0.0020
309.368	74.1	8.72	1.42	0.0031	302.052	91.3	10.03	1.79	0.0027
308.879	80.1	9.43	1.34	0.0040	301.044	97.1	10.67	1.59	0.0033
308.374	84.0	9.88	1.17	0.0047	300.540	99.8	10.97	1.45	0.0036
307.471	91.8	10.80	0.87	0.0063	300.035	106.3	11.68	1.34	0.0045
307.265	94.4	11.11	0.76	0.0069	299.530	112.0	12.31	1.18	0.0053
306.955	98.4	11.58	0.62	0.0079	299.027	118.5	13.03	0.96	0.0063
306.863	105.3	12.38	0.30	0.0098	298.774	119.5	13.13	0.80	0.0065
					298.521	122.7	13.48	0.63	0.0070
					298.269	126.7	13.92	0.40	0.0078
					298.175	129.1	14.19	0.29	0.0083
					298.095	132.4	14.55	0.15	0.0089

the critical composition of the liquid mixture situated on top of a 2 nm thick SiO_2 film [51]. This is a rather complex calculation which integrates over the dispersion dielectric data of the system [33,47]. Figure 6 demonstrates that in the region of interest ($L\sim10$ nm) $\omega_{DLP}\simeq W_{DLP}/L^2$ (dashed line) and a nonretarded dispersion interaction is appropriate. W_{DLP}, which is listed in Table II, provides a good estimate for the Hamaker constant W that appears in Eq. (14) if the adsorbed film *completely wets* the Si substrate. Our actual measurements for W (Table II) are significantly smaller than W_{DLP}. We believe that this is because our adsorbed films only partially wet the Si wafer surface, as indicated by the contact angle measurements (Φ in Table II), which were obtained photographically after dipping the Si wafer into the

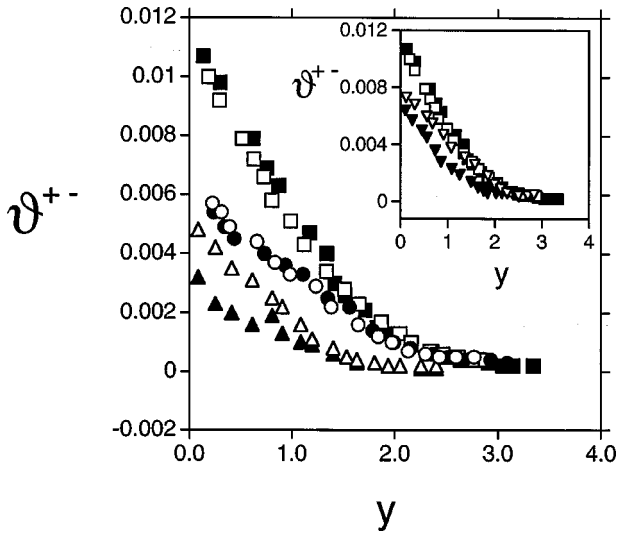

FIG. 9. Variation of $\vartheta^{+-}(y)$ for the MH system in the one-phase region as a function of composition for the critical mixture (squares), 5% excess hexane (circles), 10% excess hexane (triangles), and 5% excess methanol (inverted triangles) at two heights $H\sim 3.5$ mm (open symbols) and ~ 6.0 mm (solid symbols). Scaling is no longer observed for 10% excess hexane or 5% excess methanol.

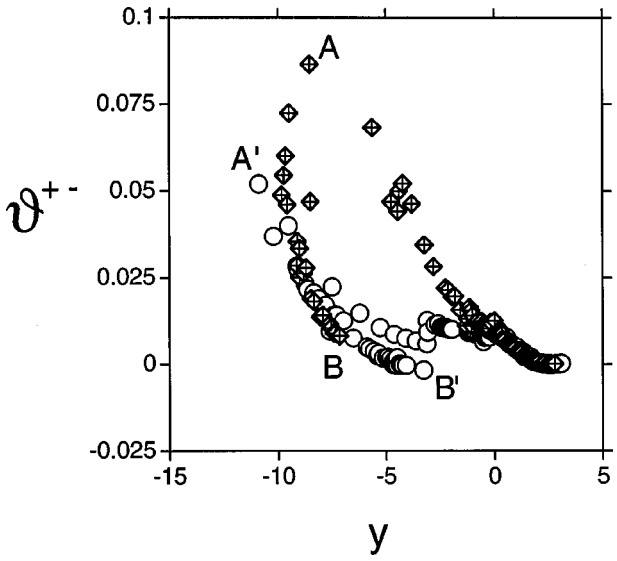

FIG. 10. The Casimir pressure scaling function $\vartheta^{+-}(y)$ obtained for a horizontal Si wafer in the one-phase ($y>0$) and two-phase ($y<0$) regions where the effective Hamaker constant W has been scaled to provide agreement with the universal scaling function obtained for a vertical Si wafer (Fig. 8) in the one-phase region. The behavior of $\vartheta^{+-}(y)$ is rather complicated in the two-phase region. The points A,B and A',B' illustrate how the data in Fig. 4 are transformed into the data in this figure. The behavior of the MM data between $y=0$ and A appears to follow the same trend established for ϑ^{+-} in the one-phase region; this suggests that the adsorbed film along this line is probably near the critical composition. Below the peak at A, the data between A and B for MM follow quite a different trend. The MH data cross over to the AB curve at the point A' so that the data between A' and B' scale in the same way as the AB curve. We believe that the scaling behavior exhibited by the curve $AB/A'B'$ corresponds to an adsorbed film possessing a composition, near the bulk phase, that is rich in the component that preferentially adsorbs against the Si wafer.

critical liquid mixture. Perhaps, therefore, it is better to call W an effective Hamaker constant.

The system-dependent parameters for both mixtures are listed in Table II and therefore the universal scaling function $\vartheta^{+-}(L/\xi_{\pm})$ can be determined using Eq. (14) by studying the adsorption thickness L as a function of T (at fixed H). Figure 7 shows L versus $\Delta T=T-T_c$ collected from a vertical Si wafer in the one-phase region of each mixture [49]. These are our best data, which provide the most consistent determination of $\vartheta^{+-}(y)$ in the one-phase region (Fig. 8) obtained by substituting the data in Fig. 7 into Eq. (14). We therefore provide these data in the form of a table (Table III) for the benefit of the reader. In Fig. 8, ϑ^{+-} scales with $y=L/\xi_{+}$ as predicted theoretically. At $y=0$ $\vartheta^{+-}(0)=2\Delta^{+-}$ and therefore $\Delta^{+-}\sim 0.0053$. This Casimir amplitude is approximately two orders of magnitude smaller than expected (Table I). In the inset to Fig. 8 we compare the scaling function $\vartheta^{+-}(y)$ for $A=0$ (crosses) and A given by Table II (squares) for the MM data at a height of $H=3.3$ mm. This inset demonstrates that the structural contribution does not significantly influence the determination of $\vartheta^{+-}(y)$. Structural contributions are only important for $T\gg T_c$ provided $L\lesssim\delta$.

In Fig. 9 we show the variation in ϑ^{+-} for MH in the one-phase region as a function of the bulk composition for two different heights H. In the analysis of the $\overline{\rho}$ data for each composition the parameters W, A, and δ were redetermined (Table IV); however, ξ_{0+} was assumed to retain the value given in Table II. From Fig. 9 scaling is no longer observed for 10% excess hexane or 5% excess methanol in the bulk mixture; scaling is observed only for compositions near the bulk critical composition as predicted by theory. This figure also indicates that our experimental value for $\Delta^{+-}\sim 0.0053$ cannot vary significantly in magnitude from this value. These off-critical effects (Fig. 9) can perhaps be taken into account using a second scaling argument $\delta\mu L^{\beta\delta/\nu}$ in the scaling function ϑ^{+-} where $\delta\mu$ denotes the undersaturation [10].

TABLE IV. Off-critical liquid mixture properties for MH.

	T_s (K)	m_H[a]	ϵ[b]	ξ_{0+} (nm)	$10^{24}W$ (J)	δ (nm)	A (J/m^2)
5% excess hexane	306.37	0.706	1.850	0.30	0.8	0.55	1.16×10^{-7}
10% excess hexane	306.07	0.740	1.856	0.30	0.7	0.55	5.10×10^{-7}
5% excess methanol	306.27	0.656	1.844	0.30	0.7	0.55	1.16×10^{-7}

[a]Mass fraction of hexane.

[b]Optical dielectric constant of the liquid mixture.

It is more difficult to quantitatively analyze the adsorption film thickness data collected from a horizontal Si wafer because W, A, and δ cannot be independently measured and the height H is less well determined. Nevertheless, we attempt an approximate analysis here. The two-phase region for the liquid mixtures MH and MM has been studied only on these horizontal wafers. In Fig. 10 we have taken the data from Fig. 4 (for a horizontal Si wafer) and rescaled the effective Hamaker constant W so that ϑ^{+-}, derived from these data, provides the best agreement with Fig. 8 (obtained from a vertical Si wafer). These values for W are also listed in Table II; they agree reasonably well with the values obtained from a vertical Si wafer. One should not expect exact agreement because the wettability of the horizontal and vertical Si wafers may differ. In Fig. 11 for $y \geqslant 0$ one observes that the horizontal and vertical Si wafers exhibit similar shapes for the scaling function ϑ^{+-}; for clarity we have plotted data from the vertical Si wafer only for the mixture MM at a height of $H=3.3$ mm. We have also plotted for comparison a rescaled mean-field scaling curve for $\vartheta^{+-}(y)$ (solid line). The mean-field scaling function (Fig. 1) was rescaled in the vertical direction to provide agreement with the experimental value for $\Delta^{+-} \sim 0.0053$ at $y=0$ and rescaled in the horizontal direction so that $y=L/\xi_{+}$ correctly exhibits an Ising critical exponent in $d=3$ (i.e., $\nu=0.632$). The mean-field result neglects fluctuations; hence we should not expect it to provide good agreement with experiments close to T_c. In fact, this modified mean-field estimate for ϑ^{+-} provides quite a different dependence on y compared with experiment for all values of y.

The scaling function for ϑ^{+-} below T_c $(y<0)$ is rather complicated (Fig. 10). We have used the universal amplitude ratio $R_{\xi}=\xi_{0+}/\xi_{0-}=1.95$ [52] in obtaining these data. There seem to be three possible types of behavior for the adsorbed film in the two-phase region: (i) the film could remain close to the bulk critical composition as expected by theory [25,32] for films possessing asymmetric boundary conditions, (ii) there could be phase separation and droplet formation on the Si wafer, and (iii) one of the two bulk phases could preferentially adsorb against the Si wafer. For the MH mixture the data is noisier near $T \sim 303$ K (Fig. 4), as noted in [49], where it was suggested that this behavior could correspond to the formation of droplets on the Si wafer. These ''droplets,'' for example, could correspond to the coexistence of two regions of differing composition and thickness on the Si wafer, where one region possesses a composition near the bulk critical composition and the other region possesses a composition near one of the bulk liquid compositions. In order to better understand the two-phase region one must compare Fig. 4 with Fig. 10. The points labeled $A,B(A',B')$ for MM (MH) are identical in both figures; these points assist the reader in understanding how the data in Fig. 4 are transformed into the data in Fig. 10. There seem to be two rather different trends in the behavior when $y<0$ (Fig. 10). The MM data from T_c $(y=0)$ up to the peak at A appear to be a continuation of the one-phase data, which would imply that these data represent an adsorbed film with a composition near the critical composition. However, below the peak, between the points A and B, ϑ^{+-} follows quite a different trend; hence the film in this region is probably no longer near the critical composition. The MH system follows a slightly different path in the two-phase region. Between T_c and the peak at A' the function ϑ^{+-} for this mixture crosses over to the lower curve represented by AB; below the peak at A' there is very good agreement between the $A'B'$ curve for MH and the AB curve for MM for the function ϑ^{+-}. As mentioned previously, the composition of the adsorbed film corresponding to the curve $AB/A'B'$ is probably rather different from the bulk critical composition. There are two likely candidates for the composition of this adsorbed film, namely, the compositions of the two bulk liquid phases. It seems probably that the curve $AB/A'B'$ represents an adsorbed film with a composition near the bulk phase rich in the component that preferentially adsorbs against the Si wafer. For MH this is the methanol-rich phase, while for MM it is the 2-methoxyethanol-rich phase. For the benefit of the reader we provide ϑ^{+-} for the curve $AB/A'B'$ in Table V.

Similar behavior to that represented by Fig. 10 has been observed by Parry and Evans [56] in their theoretical studies of a critical fluid confined between two walls possessing opposite boundary conditions. They observed an interface localization-delocalization transition at T_{cL}, the critical temperature for a system of finite size L, where in the region $T_{cL}<T<T_c$ a fluctuating interface is centered in the middle of the film while for $T<T_{cL}$ $(<T_w$, the bulk wetting transition for a semi-infinite system) the interface is bound to either one of the two walls (and two states coexist). This behavior was later confirmed in an extensive series of Monte Carlo simulations [32,57]. In Fig. 10 the curve between $y=0$ and A would correspond to a fluctuating interface in the middle of the adsorbed film, while the curve $AB/A'B'$ would represent the state below the localization-delocalization transition at T_{cL}. According to this picture, the differing locations of the localization-delocalization transition for MH and MM would originate from differing values for the bulk wetting transition T_w of the semi-infinite system.

VI. CONCLUSION

In this publication we have studied critical finite-size effects in vapor adsorbed films on molecularly smooth Si wafers suspended above a critical binary liquid mixture. We have chosen to study systems that exhibit opposite boundary conditions $(+-)$ within the adsorbed film, because for these types of films we expect the critical finite-size effects to be large. We have determined the critical Casimir pressure scaling function ϑ^{+-} using Eq. (14) for two different liquid mixtures, methanol + hexane and 2-methoxyethanol + methylcyclohexane, and shown that this function (i) is positive, which thickens an adsorbed film in the vicinity of T_c, and (ii) exhibits universal scaling as a function of the variable $y=L/\xi_{\pm}$. Both of these observations are in agreement with theoretical expectations. The universal scaling behavior is particularly obvious in the one-phase region of the mixture (Figs. 8 and 11). In the two-phase region of the mixture (Fig. 10, $y<0$) there appear to be two solutions: (i) a solution that continues the trend set by the one-phase data (from $y=0$ to the point A in Fig. 10), which we assume corresponds approximately to an adsorbed film close to the bulk critical composition, and (ii) a solution that the data follow at low temperatures below the peaks A and A' of Fig. 4. Both of the liquid mixtures exhibit the same scaling behavior in this re-

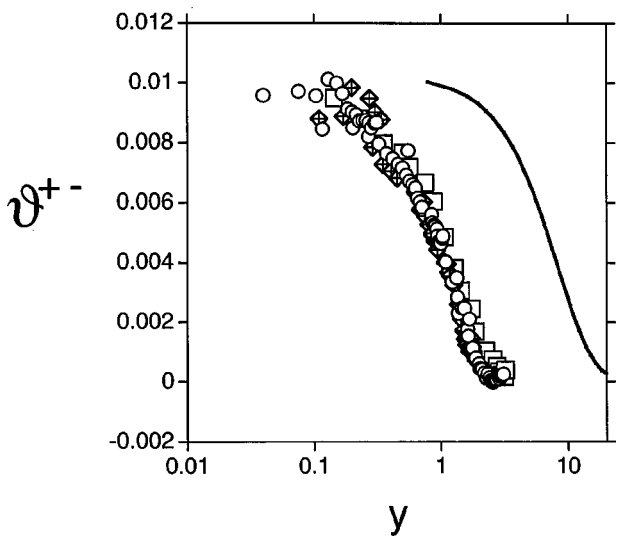

FIG. 11. Comparison between the Casimir pressure scaling function ϑ^{+-} obtained from the horizontal Si wafer [MH (circles) and MM (crossed diamonds)] and the vertical Si wafer [MM (squares) for $H=3.3$ mm]. This scaling function is also compared with the mean-field calculation from Fig. 1 (solid line), where the vertical scale for the theoretical profile has been adjusted to provide agreement at $y=0$ while the horizontal scale has been adjusted to provide the appropriate three-dimensional scaling behavior (i.e., $\nu=0.632$).

gion (AB and $A'B'$ in Fig. 10). We speculate that the universal $AB/A'B'$ curve corresponds to an adsorbed film possessing a composition near one of the bulk liquid phases; the most likely candidate is probably the bulk phase that is rich in the component that preferentially adsorbs against the Si wafer. However, additional experimental work will be required to confirm this speculation. This crossover, in the region $y<0$, from a film close to the critical composition to a film near one of the bulk phases seems to be in qualitative agreement with the ''interface localization-delocalization transition'' of [32,56,57].

Although this study has been reasonably successful in qualitatively confirming a number of features predicted by theory, the experiments also exhibit significant quantitative discrepancies with predictions. At the critical temperature T_c we find that the universal Casimir amplitude $\Delta^{+-}=\vartheta^{+-}(0)/2$ (~ 0.0053) is at least two orders of magnitude smaller than theoretical expectations for Δ^{+-}, which lie in the range 0.29 to 3.1 [16,25,26]. There are a number of deficiencies with both experiment and theory that hopefully in the future will resolve this disagreement. In the experiments the adsorbed films partially wet the Si wafer so that the contact angle $\Phi>0°$ and the effective Hamaker constant W is much smaller than the value calculated from the DLP dispersion theory, W_{DLP} (Table II). The theoretical calculation of W in the partial wetting regime appears to be not well understood. It would be more satisfying if the adsorbed film was in the complete wetting regime ($\Phi=0°$) so that $W=W_{DLP}$. This would simplify our understanding of the noncritical background term ω_{nc} [Eq. (12)] and ensure that no peculiar effects were entering because we are in the partial wetting regime. We are pursuing further experiments along these lines by studying critical finite-size effects for completely wetting films where $\Phi=0°$. We note that from a theoretical point of view the universal amplitude Δ^{+-} is not expected to be influenced by whether the adsorbed film is in the partial or complete wetting regime [58].

On the theoretical front, there have been numerous attempts to calculate the free energy contribution from *other types of fluctuations* that occur in thin films, such as acoustic fluctuations and constrained capillary wave fluctuations

TABLE V. Two-phase data.

$y=\frac{L}{\xi_-}$	ϑ^{+-}	$y=\frac{L}{\xi_-}$	ϑ^{+-}	$y=\frac{L}{\xi_-}$	ϑ^{+-}	$y=\frac{L}{\xi_-}$	ϑ^{+-}
			MH (curve AB)				
−9.83	0.0488	−9.10	0.0355	−8.49	0.0469	−7.54	0.0105
−9.73	0.0545	−9.01	0.0251	−8.47	0.0191	−7.39	0.0091
−9.64	0.0601	−9.00	0.0335	−8.34	0.0182	−7.34	0.0089
−9.56	0.0461	−8.81	0.0263	−8.03	0.0137		
−9.48	0.0724	−8.70	0.0279	−7.91	0.0142		
−9.12	0.0286	−8.52	0.0866	−7.60	0.0116		
			MH (curve $A'B'$)				
−10.88	0.0520	−7.60	0.0096	−5.14	0.0018	−4.54	−0.0001
−10.20	0.0370	−7.47	0.0125	−4.98	0.0020	−4.53	0.0010
−9.12	0.0284	−7.45	0.0141	−4.92	0.0020	−4.51	0.0004
−9.06	0.0273	−7.29	0.0142	−4.86	0.0012	−4.50	−0.0002
−8.74	0.0233	−6.96	0.0126	−4.80	0.0016	−4.49	0.0019
−8.62	0.0217	−6.52	0.0076	−4.68	0.0008	−4.38	0.0002
−8.33	0.0206	−5.88	0.0051	−4.68	0.0000	−4.31	0.0001
−8.30	0.0187	−5.76	0.0045	−4.64	0.0002	−4.22	−0.0003
−8.13	0.0190	−5.55	0.0038	−4.60	0.0013	−4.07	−0.0003
−7.87	0.0153	−5.41	0.0025	−4.60	0.0011		
−7.79	0.0171	−5.35	0.0031	−4.60	0.0000		

[59–61], which will be present even for films far from T_c. Although these contributions must be present, a complete theoretical understanding does not yet seem to be available; it is not understood when these other types of fluctuation play a major role in determining the adsorption film thickness. Various experiments have found quantitative agreement with the DLP theory for the dispersion interaction [36,62,63], while other experiments have found quantitative disagreement with this theory [63,64]. Panella, Chiarello, and Krim [63] suggest that the discrepancies with DLP theory can be attributed to properties of the adsorbate rather than the substrate while Mecke and Krim [61] provide evidence that the constrained capillary wave contribution is particularly important for very thin adsorbed films ($\lesssim 5$ nm). Unfortunately, many of the experiments that claim disagreement with the DLP theory have not demonstrated that the adsorbed film, in fact, completely wets the substrate so that we can take $W = W_{DLP}$. If a constrained capillary wave free energy term does play an important role for thin films, then it could potentially influence the value of the Casimir amplitude Δ^{+-}. Another alternative possibility that needs to be considered in more detail and that could produce a large difference between the experimental value for Δ^{+-} and theory is the coupling between the gravitational field and the order parameter (because the two phases do not have exactly the same density) [16]; hence, in this case, the ordering field does not vanish at the critical point.

ACKNOWLEDGMENTS

This research work has been supported by the National Science Foundation through Grant No. DMR-9631133. We would like to thank Professor S. Dietrich for both suggesting this experiment and providing us with valuable advice. We would also like to thank Dr. M. Krech for enlightening communications and publications and Professor R. Evans for useful discussions.

[1] H. B. G. Casimir, Proc. K. Ned. Akad. Wet. **51**, 793 (1948).
[2] E. M. Lifshitz, Zh. Éksp. Teor. Fiz. **29**, 94 (1955) [Sov. Phys. JETP **2**, 73 (1956)].
[3] I. E. Dzyaloshinskii, E. M. Lifshitz, and L. P. Pitaevskii, Adv. Phys. **10**, 165 (1961).
[4] M. Kardar and R. Golestanian, Rev. Mod. Phys. **71**, 1233 (1999).
[5] M. E. Fisher and P. G. de Gennes, C. R. Seances Acad. Sci., Ser. B **287**, 207 (1978).
[6] M. E. Fisher, in *Critical Phenomena*, Proceedings of the 1970 International School of Physics ''Enrico Fermi,'' Course LI, edited by M. S. Green (Academic, New York, 1971); M. E. Fisher and M. N. Barber, Phys. Rev. Lett. **28**, 1516 (1972).
[7] M. Krech, *The Casimir Effect in Critical Systems* (World Scientific, Singapore, 1994).
[8] M. N. Barber, in *Phase Transitions and Critical Phenomena*, edited by C. Domb and J. L. Lebowitz (Academic, London, 1983), Vol. 8.
[9] V. Privman, P. C. Hohenberg, and A. Aharony, in *Phase Transitions and Critical Phenomena*, edited by C. Domb and J. L. Lebowitz (Academic, New York, 1991), Vol. 14.
[10] M. Krech, J. Phys.: Condens. Matter **11**, R391 (1999).
[11] W. A. Ducker, T. J. Senden, and R. M. Pashley, Nature (London) **353**, 239 (1991); Langmuir **8**, 1831 (1992); A. Milling, P. Mulvaney, and I. Larson, J. Colloid Interface Sci. **180**, 460 (1996).
[12] J. N. Israelachvili and P. M. McGuggian, Science **241**, 795 (1988).
[13] M. Krech and S. Dietrich, Phys. Rev. A **46**, 1886 (1992).
[14] P. G. de Gennes, Rev. Mod. Phys. **57**, 827 (1985).
[15] J. N. Israelachvili, *Intermolecular and Surface Forces*, 2nd. ed. (Academic, London, 1991).
[16] M. P. Nightingale and J. O. Indekeu, Phys. Rev. Lett. **54**, 1824 (1985); **55**, 1700 (1985); J. O. Indekeu, M. P. Nightingale, and W. V. Wang, Phys. Rev. B **34**, 330 (1986).
[17] M. Krech and S. Dietrich, Phys. Rev. Lett. **66**, 345 (1991); **67**, 1055 (1991); Phys. Rev. A **46**, 1886 (1992).
[18] H. W. Diehl, in *Phase Transitions and Critical Phenomena*, edited by C. Domb and J. L. Lebowitz (Academic, London, 1986), Vol. 10, p. 76.
[19] T. W. Burkhardt and H. W. Diehl, Phys. Rev. B **50**, 3894 (1994).
[20] H. E. Stanley, *Introduction to Phase Transitions and Critical Phenomena* (Oxford Universityy Press, New York, 1971).
[21] A. J. Liu and M. E. Fisher, Phys. Rev. A **40**, 7202 (1989).
[22] B. M. Law, Ber. Bunsenges. Phys. Chem. **98**, 472 (1994); Phys. Rev. E **48**, 2760 (1993).
[23] H. Au-Yang and M. E. Fisher, Phys. Rev. B **21**, 3956 (1980); Physica A **101**, 255 (1980).
[24] J. S. Rowlinson and B. Widom, *Molecular Theory of Capillarity* (Clarendon, Oxford, 1982).
[25] M. Krech, Phys. Rev. E **56**, 1642 (1997).
[26] Z. Borjan and P. J. Upton, Phys. Rev. Lett. **81**, 4911 (1998).
[27] H. W. Blöthe, J. L. Cardy, and M. P. Nightingale, Phys. Rev. Lett. **56**, 742 (1986); J. L. Cardy, Nucl. Phys. B **275**, 200 (1986).
[28] Note that for the upper critical dimension $d=4$ an extra logarithmic divergence occurs in L so that $\omega_c/kT = \Delta^{ab} L^{-3} \ln L$ at T_c, which is somewhat different from what would be obtained from Eq. (3) [25,26].
[29] R. Evans and J. Stecki, Phys. Rev. B **49**, 8842 (1994).
[30] N. B. Wilding and M. Krech, Phys. Rev. E **57**, 5795 (1998).
[31] R. Garcia and M. H. W. Chan, Phys. Rev. Lett. **83**, 1187 (1999).
[32] K. Binder, D. P. Landau, and A. M. Ferrenberg, Phys. Rev. Lett. **74**, 298 (1995); Phys. Rev. E **51**, 2823 (1995).
[33] J. Mahanty and B. W. Ninham, *Dispersion Forces* (Academic, London, 1976).
[34] D. B. Hough and L. R. White, Adv. Colloid Interface Sci. **14**, 3 (1980).
[35] N. V. Churaev and B. V. Derjaguin, J. Colloid Interface Sci. **103**, 542 (1985).
[36] E. S. Sabisky and C. H. Anderson, Phys. Rev. A **7**, 790 (1973); R. F. Kayser, J. W. Schmidt, and M. R. Moldover, Phys. Rev. Lett. **54**, 707 (1985).
[37] W. Kern and D. A. Puotinen, RCA Rev. **31**, 187 (1970).

[38] L. Holland, *The Properties of Glass Surface* (Chapman and Hall, London, 1964).
[39] J. Vig, J. Vac. Sci. Technol. A **3**, 1027 (1985).
[40] A glass etch consisting of 5% HF, 35% HNO_3, and 60% H_2O by volume was used as recommended in Ref. [38].
[41] D. Beaglehole, Physica B & C **100B**, 163 (1980).
[42] D. Beaglehole, in *Fluid Interfacial Phenomena*, edited by C. A. Croxton (Wiley, New York, 1986).
[43] B. M. Law and H. K. Pak, J. Opt. Soc. Am. A **13**, 379 (1996).
[44] All the chemicals were purchased from Aldrich Chemical company and used as received. The quoted purity for hexane and methylcyclohexane is 99%, while for 2-methoxyethanol and methanol, it is 99.9+%.
[45] R. M. A. Azzam and N. M. Bashara, *Ellipsometry and Polarized Light* (North-Holland, Amsterdam, 1987).
[46] P. Drude, *The Theory of Optics* (Dover, New York, 1959).
[47] R. F. Kayser, Phys. Rev. B **34**, 3254 (1986).
[48] M. Born and E. Wolf, *Principles of Optics*, 6th (corrected) ed. (Pergamon, Oxford, 1980); B. M. Law and D. Beaglehole, J. Phys. D **14**, 115 (1981).
[49] A. Mukhopadhyay and B. M. Law, Phys. Rev. Lett. **83**, 772 (1999).
[50] ξ_{0+} is determined using the method given by D. S. P. Smith, B. M. Law, M. Smock, and D. P. Landau, Phys. Rev. E **55**, 620 (1997), where the revised value of $(\xi_+/\lambda)_{peak}=0.064 \pm 0.006$ from J. H. Carpenter, B. M. Law, and D. S. P. Smith, *ibid.* **59**, 5655 (1999) is used in the calculation.
[51] V. A. Parsegian and B. W. Ninham, J. Theor. Biol. **38**, 101 (1973).
[52] We have assumed an average value near theoretical estimates for the ''true correlation length'' [53] and the ''second moment of the bulk correlation length'' [54,55]; however, we note that recently Floter and Dietrich [55] determined rather a different value for the ''true correlation length,'' $R_\xi=1.73 \pm 0.04$, from an interpolation of exact results in two and four dimensions to three dimensions.
[53] H. B. Tarko and M. E. Fisher, Phys. Rev. Lett. **31**, 926 (1973).
[54] A. J. Liu and M. E. Fisher, Physica A **156**, 35 (1989); C. Ruge, P. Zhu, and F. Wagner, *ibid.* **209**, 431 (1994).
[55] G. Flöter and S. Dietrich, Z. Phys. B: Condens. Matter **97**, 213 (1995).
[56] A. O. Parry and R. Evans, Phys. Rev. Lett. **64**, 439 (1990); Physica A **181**, 250 (1992).
[57] K. Binder, P. Nielaba, and V. Pereyra, Z. Phys. B: Condens. Matter **104**, 81 (1997).
[58] S. Dietrich (private communication).
[59] N. K. Mahale and M. W. Cole, Surf. Sci. **172**, 311 (1986).
[60] A. A. Chernov and L. V. Mikheev, Dokl. Akad. Nauk (SSSR) **297**, 349 (1987) [Sov. Phys. Dokl. **32**, 906 (1987)]; L. V. Mikheev, Pis'ma Zh. Éksp. Teor. Fiz. **47**, 147 (1988) [JETP Lett. **47**, 178 (1988)]; Phys. Lett. A **129**, 245 (1988).
[61] K. R. Mecke and J. Krim, Phys. Rev. B **53**, 2073 (1996).
[62] B. M. Law, Phys. Rev. E **50**, 2827 (1994).
[63] V. Panella, R. Chiarello, and J. Krim, Phys. Rev. Lett. **76**, 3606 (1996), and references therein.
[64] D. Beaglehole, E. Z. Radlinska, B. W. Ninham, and H. K. Christenson, Phys. Rev. Lett. **66**, 2084 (1991).